A mass threshold in the number density of passive galaxies at z~2

V. Sommariva[1], A. Fontana[1], A. Lamastra[1], P. Santini[1], J. S. Dunlop[3], M. Nonino[2], M. Castellano[1], H. Ferguson[4], R. J. McLure[3], A. Galametz[1], M. Giavalisco[5], A. Grazian[1], Y. Lu[6], N. Menci[1], A. Merson[7], D. Paris[1], L. Pentericci[1], R. Somerville[4], and T. Targett[3]

[1] INAF - Osservatorio Astronomico di Roma, Via Frascati 33, IÐ00040, Monteporzio, Italy e-mail: veronica.sommariva@oa-roma.inaf.it
[2] INAF - Osservatorio Astronomico di Trieste, Via G.B. Tiepolo 11, 34131 Trieste, Italy.
[3] SUPA, Institute for Astronomy, University of Edinburgh, Royal Observatory, Edinburgh, EH9 3HJ, UK
[4] Space Telescope Science Institute, 3700 San Martin Dr., Baltimore, MD 21218, USA
[5] Astronomy Department, University of Massachusetts, Amherst, MA 01003, USA
[6] kavli institute for particle astrophysics and cosmology, 452 Lomita Mall Stanford, CA 94305-4085
[7] Department of Physics and Astronomy, University College London, Gower Street, London WC1E 6BT, UK

ABSTRACT

The process that quenched star formation in galaxies at intermediate and high redshift is still the subject of considerable debate. One way to investigate this puzzling issue is to study the number density of quiescent galaxies at $z \simeq 2$, and its dependence on mass. Here we present the results of a new study based on very deep K_s-band imaging (with the HAWK-I instrument on the VLT) of two HST CANDELS fields (the UKIDSS Ultra-deep survey (UDS) field and GOODS-South). The new HAWK-I data (taken as part of the HUGS VLT Large Program) reach detection limits of $K_s > 26$ (AB mag). We have combined this imaging with the other ground-based and HST data in the CANDELS fields to select a sample of passively-evolving galaxies in the redshift range $1.4 < z < 2.5$ (via the *pBzK* color-based selection criterion of Daddi et al. 2004). Thanks to the depth and large area coverage of our imaging, we have been able to extend the selection of quiescent galaxies a magnitude fainter than previous analyses. Through extensive simulations we demonstrate, for the first time, that the observed turn-over in the number of quiescent galaxies at $K \geq 22$ is not due to incompleteness, but is real. This has enabled us to establish unambiguously that the number counts of quiescent galaxies at $z \simeq 2$ flatten and slightly decline at magnitudes fainter than $K_s \sim 22$ (AB mag.), in contrast to the number density of star-forming galaxies which continues to rise to fainter magnitudes. We show that this trend corresponds to a stellar mass threshold $M_* \simeq 10^{10.8}$ $M_\odot$ below which the mechanism that halts the star formation in high-redshift galaxies seems to be inefficient. We also show that, while *pBzK* galaxies at $K < 23$ are in the redshift range $1.4 < z < 2.5$, as expected, at $K > 23$ a higher redshift population of $z \simeq 3$ *pBzK* galaxies is detected, and dominates the counts at the faintest magnitudes. Finally we compare the observed *pBzK* number counts with those of quiescent galaxies extracted from four different semi-analytic models. We find that only two of these models reproduce even qualitatively the observed trend in the number counts, and that none of the models provides a statistically acceptable description of the number density of quiescent galaxies at these redshifts. We conclude that the mass function of quiescent galaxies as a function of redshift continues to present a key and demanding challenge for proposed models of galaxy formation and evolution.

Key words. Galaxies: high redshift - Galaxies: fundamental parameters -

1. Introduction

The cessation, or "quenching" of star formation activity in galaxies at high and intermediate redshifts is one of the key events in the history of galaxy evolution, and one that is not easily explained in the context of hierarchical growth within a ΛCDM cosmology. While it is now established that the (apparently fairly rapid) termination of star formation in some subset of the galaxy population only a few billion years after the Big Bang must be attributed to some aspect of baryonic physics, the relevant process remains a matter of debate, with opinion divided over whether the key mechanism is feedback from an active galactic nucleus (AGN), feedback from star formation itself, or termination of the gaseous fuel supply (e.g. due to the difficulty of cool gas penetrating to the centre of a massive halo due to shock heating). Better observational constraints on the prevalence and properties of quiescent galaxies at high redshift are therefore urgently required in order to constrain models of galaxy formation and evolution over cosmic history.

One key goal is to better establish the mass dependence of star-formation quenching. A number of lines of evidence suggest that this process appears "anti-hierarchical" in the sense that it is the most massive galaxies that cease star formation at the earliest times, leading ultimately to the present-day Universe in which the most massive elliptical galaxies appear to be the oldest. However, because less-massive passive galaxies are hard to detect and isolate at high redshift (especially at optical wavelengths), it has proved difficult to establish the definitive mass dependence of the number density of passive galaxies at the crucial epoch corresponding to $z \simeq 2$. The primary aim of this study is to clarify this situation via new deep multi-frequency imaging data.

Several methods have been developed to efficiently select passively-evolving galaxies at high-redshift based on color criteria. In recent years, the most extensively used selection technique is the *BzK* color-color selection introduced by Daddi et al. (2004). They showed that galaxies in the redshift range

$1.4 < z < 2.5$ fall into a specific area of the $(B − z) / (z − K)$ diagram, and demonstrated that galaxies can be easily separated into star-forming ($sBzK$) and passively-evolving ($pBzK$) classes. This technique also has the advantage of not being biased by the presence of dust; the reddening vector in the BzK plane is parallel to the BzK selection line, making this criterion relatively immune to dust content.

A number of studies have used the BzK-criterion to constrain the properties of star-forming and passive galaxies at $z ≃ 2$. For example, Kong et al. (2006) presented K_s-selected samples of BzK galaxies over two fields: a $≃ 920$ arcmin² field (with $K_{s;AB} < 20.8$) and a $≃ 320$ arcmin² field (to $K_{s;AB} ≃ 21.8$). They particularly concentrated their analysis on the clustering properties of BzK galaxies, and concluded that the $pBzK$ galaxies are more clustered than the $sBzK$ galaxies. Meanwhile, Lane et al. (2007) combined the first release of the near-infrared UKIRT Infrared Deep Sky Survey (UKIDSS) Ultra-Deep Survey (UDS; Lawrence et al. 2007) with optical photometry from Subaru imaging. By comparing the commonly-used selection techniques for galaxies at intermediate redshift, they concluded that the brightest Distant Red Galaxies (DRG) have spectral energy distributions (SED) consistent with dusty star-forming galaxies at $z ≃ 2$. Moreover, they observed an interesting turn-over in their derived number counts of $pBzK$ galaxies at $K ≃ 21$, suggesting an absence of high-redshift passive galaxies at lower luminosities. Grazian et al. (2007), instead, focused on the overlap between DRG and BzK galaxies, discussing their relative contribution to the overall stellar mass density.

The galaxy population in the UKIDSS UDS field was also studied by Hartley et al. (2008), in order to measure the clustering properties, number counts and the luminosity function of a sample of star-forming and quiescent BzK galaxies with a limiting magnitude $K_{s;AB} < 23$. The number counts they derived for the passive objects exhibit a flattening at $K_s ≃ 21$ and an apparent turn-over at $K_s ≃ 22$: they concluded that the former effect is likely to be real, while the latter is probable but remains uncertain. More recently, McCracken et al. (2010) presented number counts and clustering properties for a sample of $pBzK$ galaxies with $K_s < 23$, selected over a significantly larger area than previous studies ($2\,\text{deg}^2$ in the COSMOS field). They also found some evidence for a turn-over in the number counts of quiescent galaxies, around $K_s ≃ 22$.

It is interesting to notice that similar conclusions were already reached by other papers using different techniques. For instance, De Lucia et al. (2007) used a combination of photometric and spectroscopic data to study the evolution of cluster environment over a large range of cosmic time, from redshift 0.4 to 1. They found a significant deficit of low mass, faint red galaxies going to high redshift. A similar conclusion, i.e. the truncation of the red sequence at faint magnitude for high redshift galaxies, was confirmed by other authors such as Kodama et al. (2004), and Andreon et al. (2011). A decline in the number density of the quiescent population at faint magnitudes was also observed in the H_{160}-band by Stutz et al. (2008). More recently, Ilbert et al. (2013) presented galaxy stellar mass functions and stellar mass densities for star-forming and quiescent galaxies in the redshift range $0.2<z<4$ using the UltraVISTA DR1 release. They studied the stellar mass function for both star forming and quiescent galaxies, and found that the number density of massive, quiescent galaxies is relatively unchanged out to high redshift. They interpreted this evidence as a direct consequence of star formation being drastically reduced or quenched when a galaxy becomes more massive than M$> 10^{10.7−10.9}$ M$_\odot$. This result is consistent with the one presented in Muzzin et al. (2013),

who also computed the stellar mass function for quiescent galaxies using the UltraVISTA data. In general, dedicated analyses of the evolution of "Red&Dead" galaxies show an evolution in the fraction of red galaxies (e.g. Fontana et al. 2009, Brammer et al. 2011), that decreases as redshift increases.

The use of the BzK selection method for finding passively evolving galaxies has the distinct advantages of being relatively easy to perform on data, of being easily and self–consistently reproducible on mock catalogs derived from theoretical simulations, and has been relatively well tested with spectroscopic follow-up. However, it is crucial to stress that the success rate of the BzK selection is strongly dependent on the availability of deep imaging at both optical and near-infrared wavelengths. All the above-mentioned surveys were limited both by the depth of the near-infrared data, and by the relative depth of the imaging in the bluer bands. The robust detection of passively-evolving BzK galaxies, requires a proper measure of a color term as large as $B − K ≃ 7$. If the B-band imaging is of limited depth, the clean selection of $pBzK$ galaxies cannot reach the faint K-band limits where the bulk of the population is expected to lie, and the observed number counts are severely prone to errors due to incompleteness and noise. Because of these limitations, the existence of a turn-over in the observed number counts of quiescent galaxies at $z ≃ 2$ has yet to be firmly established.

In this paper, we use a combination of wide-field and deep optical and infrared images that allow us to robustly select a sample of passively-evolving galaxies at $z ≃ 2$ to $K_s ≃ 25$, and to explore the dependence of the number density of these quiescent objects as a function of luminosity or, equivalently, stellar mass. The data have been acquired in the context of the CANDELS HST (Grogin et. al 2011; Koekemoer et al. 2011) and HUGS VLT (Fontana et al. 2014) surveys, that deliver a unique combination of area and depth in the the B, z and K_s bands. With this unique sample we study the number counts of the BzK galaxy population, and in particular we focus on the quiescent population to provide improved constraints on the nature of the physical processes involved in the quenching of star formation.

The paper is organized as follows: in Section 2 we describe the data and the multiwavelength catalog for the UDS and GOODS-S fields, in Section 3 we provide an updated view of the properties of faint BzK galaxies as obtained by the unique CANDELS data set, and in Section 4 we present the simulations performed to quantify the incompleteness of the observed sample. A reader less interested in the technical details may go directly to Sect. 5, where we present the crucial result of the paper, i.e. the luminosity and mass distribution of $pBzK$ galaxies, and to Sect. 6 , where we compare our results with the predictions of various semi-analytical models (SAM) of galaxy formation. Finally, a discussion of our results and a summary of our main conclusions is presented in Sec. 7.

All magnitudes utilised in the paper are in the AB system (Oke 1974) and a standard cosmological model ($H_0 = 70$ km/s/Mpc, $\Omega_M = 0.3$ and $\Omega_\Lambda = 0.7$).

2. Data

2.1. Imaging data

The present paper is based on data collected over the CANDELS pointings of the UDS and the GOODS-S fields. Both these $≃ 200\,\text{arcmin}^2$ fields have been observed in many broad bands in recent years, including WFC3/IR and ACS with the *Hubble Space Telescope* (HST), as a part of CANDELS HST Treasury Project (Grogin et al. 2011; Koekemoer et al. 2011). Additional

ultradeep images from the U to the mid-infrared Spitzer bands are also available. A complete description of the imaging data available in these fields along with the procedure adopted for catalog extraction are given in Galametz et al. (2013, G13 in the following) for UDS and in Guo et al. (2013, GUO13 in the following) for GOODS-S, respectively.

Since this work makes crucial use of the B, z and K bands to select passive galaxies, we briefly summarize here the properties of these images, including new imaging data in the B and K bands recently collected with VLT that are not included in the aforementioned catalog papers.

In the K band, the two fields have been imaged by the High Acuity Wide field K-band Imager (HAWK-I) on the European Southern Observatory's Very Large Telescope (VLT) as part of the HUGS survey (an acronym for HAWK-I UDS and GOODS-S survey). This program has delivered very deep images in the K_s band over both fields, reaching 5-σ detection limits fainter than $K_s \simeq 26$. We refer to Fontana et al. (2014) for a complete description of the HUGS survey. The K_s band of HAWK-I will be referred to simply as the K-band in the rest of this paper.

For UDS, the final K-band photometry is already included in the G13 catalog. The whole UDS field is covered with three different pointings. Their seeing is $0.37'' - 0.43''$ and the corresponding limiting magnitudes are $m_{lim}(K) \simeq 26$, $m_{lim}(Y) \simeq 26.8$ (5σ in one FWHM) or $m_{lim}(K) \simeq 27.3$, $m_{lim}(Y) \simeq 28.3$ (1σ per arcsec^2). In GOODS-S, we use here the final HUGS image, that is considerably deeper than the image used in GUO13. The whole field was covered with 6 (partly overlapping) pointings for a total exposure time in the K band (summed over the six pointings) of 107 hours. Because of the complex geometry, this corresponds to an exposure of 60–80 hours in the central area (the one covered by CANDELS "Deep") and 12–20 hours in the rest (the CANDELS "Wide" area). The final average seeing is remarkably good and constant, with 4 pointings at $0.38''$ (notably including the two deepest) and 2 pointings at $0.42''$. On the finally stacked images, the limiting magnitudes in the deepest area are $m_{lim}(K) \simeq 27.8$ (5σ in one FWHM) or $m_{lim}(K) \simeq 28.3$, $m_{lim}(Y) \simeq 28.3$ (1σ per arcsec^2).

The B and z' images in the UDS were obtained with Subaru/Suprime-Cam (see Furusawa et al. 2008). The Subaru optical data cover the full CANDELS UDS field, and the 5σ limiting magnitudes (computed in 1 FWHM of radius) are 28.38 and 26.67 in B and z' respectively (G13).

Another crucial data set in this context is a recent ultradeep B-band image obtained with VIMOS on VLT for GOODS-S (Nonino et al. in prep.). Here the average seeing is $0.89''$. With a VLT/VIMOS total integration time of 24 hr, the final mosaics have a median PSF of 0.85 arcsec FWHM, and reach $B = 28.4$ at 5σ, and are thus considerably deeper than the available ACS $F435W$ data (the latest V2.0 version released by the GOODS Team reaches a 5σ limit of $F435W \simeq 26.9$). We will use in the following this VIMOS B-band image. As for the GOODS-S z band, we used the $F850LP$ image originally obtained in the GOODS program (Giavalisco et al. 2004) and then augmented by subsequent observations. Guo et al. 2013 report a 5σ limit of $m_{AB} = 28.55$ in a small aperture of radius 0.09".

While the B, z and K bands are crucial for the selection of passive galaxies, we have also utilized the full multi-color data from the U-band to the mid-infrared Spitzer bands at various stages in our analysis, both to derive photometric redshifts and to determine the shapes of the spectral energy distributions (SEDs) of the selected galaxies. We refer to G13, GUO13, and Fontana et al. (2014) for a complete description of the imaging data set.

2.2. Catalogs

The catalogs used in this paper are those already published in G13 and GUO13, with the only notable difference that we have included the new B and K images, as described below.

The adoption of the CANDELS catalogs implies that we rely on the H_{160} band for the detection of galaxies. This choice has the practical benefit that we have been able to use the existing CANDELS catalogs, and takes full advantage of the depth and the quality of the HST images. Because the H_{160} imaging is still significantly deeper than the K-band imaging, this choice does not affect the definition of the K-selected sample; we have performed an independent detection in the K band and verified that all the objects detected in K are also detected in H-band, at least to the magnitude limits we are interested in here.

From the whole H–selected sample we have then selected the objects that fall in the regions where the K band images are well exposed, trimming the outer edges of the images. The remaining areas are 151.08 arcmin^2 in GOODS-S (defined as all pixels of the image having a 1-σ magnitude limit > 27 in one sq. arcsec) and 178.09 arcmin^2 in UDS (made by pixels with a 1-σ magnitude limit > 26.5 in one sq. arcsec). The final UDS sample (that is complete to $H \simeq 26$ and extends to $H \simeq 27$) contains 27831 H–selected objects, while the GOODS sample (that is complete to $H \simeq 26.6$ and extends to $H \simeq 28$) contains 31551 H–selected objects.

Colors in the ACS and WFC3/IR bands have been measured by running SExtractor in dual-image mode, using isophotal magnitudes (MAG_ISO) for all the galaxies, after smoothing each image with an appropriate kernel to reproduce the resolution of the H_{160} WFC3/IR image. The Template-FITting photometry software TFIT (Laidler et al. 2007) was used to derive the photometry for all the images that have poorer resolution than H_{160} (e.g. B, z' and K). This code uses information (position, profile) of sources measured on a high-resolution image (here H_{160}) as priors to establish the photometry in the lower-resolution images. We refer to G13 for a more detailed discussion of the CANDELS UDS multiwavelength catalog. For the new B and K images used here we have applied TFIT exactly as described in G13 and GUO13.

We remark that the TFIT code that we used to measure colors is designed to minimize the effects of blending from nearby sources when extracting the photometry of faint sources in crowded extragalactic fields. The power of TFIT in this context is clearly shown by the simulations presented in Lee et al. (2012), where it is shown that the contamination from nearby sources is minimal even in the case of the $\simeq 3''$ PSF of the Spitzer images. The ground–based images on which this analysis is based (B, z, K) have a much smaller PSF, especially in K where the seeing is consistently better than $0.45''$, and we therefore expect possible contaminations to be even smaller. As a further check, we have verified that only 5% of galaxies at $K \simeq 23.5 - 24$ (the most typical objects that we target) have a nearby brighter companion within $2''$, that may be affecting the measured colors. We are therefore confident that our results are not significantly affected by photometric contamination.

We also note that the images used in this analysis are remarkably homogeneous in depth over the area that we use. Ground–based B and z images have been obtained with imagers with FOV larger than those of CANDELS fields, and the dithering pattern adopted for Hawk–I has ensured a proper coverage of the full area. We have explicitly verified this by looking at the distributions of the 1–σ magnitude limits in the B, z and K images for our BzK galaxies, and we verified that they are reasonably nar-

row gaussian distributions. The remaining inhomogeneities are accounted for in the simulations that we used to evaluate the systematics in our analysis.

To facilitate comparison of our results with previous studies we wanted our photometric selection criterion to match as closely as possible the original *BzK* selection introduced in Daddi et al. (2004). Since the filters used here in both the GOODS-S and UDS fields are not identical to those used in the original *BzK* paper, we computed the correction term to the colors to account for the different shape of the filters. Correction terms were computed using synthetic models of Galactic stars, and checked against the terms computed with the Bruzual & Charlot (2003) (BC03) evolutionary synthesis code. Corrections for the two colors in GOODS-S and for $z - K$ in UDS turned out to be relatively small, nearly always less than 0.05 mag, both between the UDS and GOODS-S filters, as well as in comparison with the original Daddi et al. photometry. The $(B - z)$ color term in UDS turned out to be significantly larger, with a strong linear trend up to $\Delta(B - z)_{UDS-GOODS-S} \simeq \Delta(B - z)_{UDS-Daddi} \simeq -0.3$. We therefore decided to apply only a correction to $(B - z)_{UDS}$, in order to bring it as close as possible to $(B - z)_{GOODS}$, neglecting all the other much smaller color terms. The corrected color is $(B - z)_{UDS}^{corr} = (B - z)_{UDS} + 0.135 \times (B - z)_{UDS} + 0.045$ up to $(B - z)_{UDS} = 2$, and $(B - z)_{UDS}^{corr} = (B - z)_{UDS} + 0.315$ at larger $(B - z)_{UDS}$. Hereafter we will apply this correction to data and theroretical models (when computed explicitly in the UDS filter set) and refer to $(B - z)_{UDS}^{corr}$ as $(B - z)_{UDS}$ for simplicity. The final agreement can be visualized in Figure 1, where we have plotted an identical red dashed line in the two panels that overlaps the stellar loci of the two fields. As can be seen, the consistency of the two calibrations is good.

2.3. The SED fitting

While the selection of passive galaxies is performed using only the *BzK* bands, we exploit the full multiwavelength catalogs delivered by CANDELS to obtain further information on the targeted galaxies, including photometric redshifts, stellar masses and other quantities.

For all the *BzK* galaxies without a secure spectroscopic redshift we used the official photometric redshift produced by the CANDELS collaboration. The technique adopted is described in Dahlen et al. (2013), and photometric redshifts for both fields will be made available in forthcoming papers (Dahlen et al., in prep.). For the sample of *BzK* galaxies with secure spectroscopic redshifts we find that the scatter between photometric and spectroscopic redshifts is gaussian distributed, with a standard deviation $\sigma \sim 0.08$ and a small number of outliers, about 5%.

To compute the physical parameters of the galaxies we used a SED fitting technique applied on the full multiwavelength catalog available for the two CANDELS fields, that have 18/19 bands on UDS/GOODS, from U-band to $8\mu m$. The SED technique employed for this work has been already intensively tested in previous papers (Fontana et al. 2003, 2004, 2006; Grazian et al. 2006; Santini et al. 2012). It is based on the comparison between the observed multi-color SED of each galaxy with those obtained from a set of reference synthetic spectra from stellar population models. The redshift of each galaxy is fixed to the spectroscopic or the photometric one during the fitting process.

We decided in this case to use a fairly standard reference spectral library, to facilitate comparison with results in the literature. It is based on the BC03 models, and the code was run using a Salpeter IMF, ranging over a set of metallicities from $Z = 0.02 Z_{\odot}$ to $Z = 2.5 Z_{\odot}$, and dust extinction A_V ranging

Table 1. Parameters used for the library of template SEDs.

IMF	Salpeter
SFR τ (Gyr)	0.1,0.3,0.6,1,23,4,9,15
log (age) (yr)	7, 7.01, 7.03...10.3
Metallicities	0.02 $Z_{\odot}$, 0.2$_{\odot}$, 1$_{\odot}$, 2.5$_{\odot}$
E_{B-V}	0, 0.03, 0.06, 0.1, 0.15, 0.2, ..., 1.0
Extinction law	SMC, Calzetti

between 0 and 1.0 assuming a Calzetti extinction curve. We used smooth exponentially-decreasing star-formation histories. All the parameters adopted for the SED fitting are listed in Tab. 1. The best-fitting spectrum provides estimates of the star-formation rate (SFR), extinction, stellar population age (the onset of the star formation episode) and galaxy stellar mass, and τ (the star-formation e-folding timescale).

Among the outputs of this analysis we will use in particular the stellar masses and the age/τ parameter, that is the inverse of the Scalo parameter. As shown in Grazian et al. (2007), this parameter can be used to discriminate between star forming and passively evolving galaxies. Following their work, we assume age/$\tau < 4$ for the former and age /$\tau \geq 4$ for the latter.

3. *BzK* galaxies in CANDELS

3.1. Raw *BzK* counts

As first proposed by Daddi et al. (2004), the *BzK* color-color criterion is an efficient color-based method for identifying galaxies in the redshift range $1.4 < z < 2.5$. It also permits segregation of galaxies between actively star-forming galaxies (*sBzK*) and passively-evolving galaxies (*pBzK*). If we define $BzK = (z - K) - (B - z)$, *sBzK* galaxies have colors consistent with $BzK > -0.2$ while *pBzK* galaxies have $BzK < -0.2$ and $(z - K) > 2.5$ (corresponding to the upper-left and upper-right regions of the color-color diagram respectively; see Figure 1).

Figure 1 shows the $B - z$ versus $z - K$ distribution of $K \leq 24$ sources in the CANDELS GOODS-S (upper panel) and UDS (lower panel) fields. While all *BzK* galaxies are detected in the z-band images, the same does not hold for the B band, where several of them are undetected even in our ultradeep images. We assume for these sources a lower limit on B-band magnitude equal to their 1σ limiting magnitude, and plot them as horizontal arrows in Figure 1. We note that, in principle, *BzK* galaxies undetected in the B band and located in the *sBzK* region could be *pBzK* galaxies scattered left-ward into the *sBzK* region, as shown also in Grazian et al. (2007), which therefore escape inclusion in the *pBzK* sample.

Based on our sample, we are able to compute the raw number counts derived for both the *sBzK* and *pBzK* galaxies in the CANDELS fields for both fields separately, as shown in Figure 2. The error bars are computed assuming Poisson statistics, approximated with the square root of the counts for $N > 10$ and the small-number approximation for the Poisson distribution of Gehrels (1986) for $N \leq 10$. It is immediately clear that our observations reach a depth that no previous studies have achieved. Also evident is the decrease in the number counts of *pBzK* galaxies at magnitudes fainter than $\simeq 21.5 - 22$. To establish whether this turnover is real we have performed dedicated simulations that are described in the following section.

The number counts for star-forming and passive *BzK* galaxies are reported in Table 2 and Table 3, respectively. Since the detection is made on the deep *H*-band CANDELS images, the
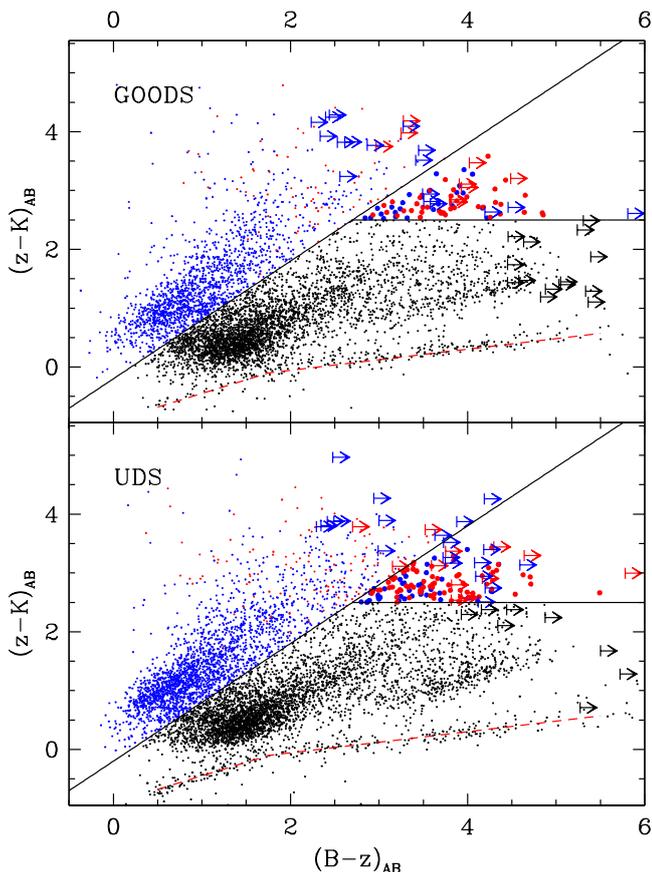
Fig. 1. $B-z$ versus $z-K$ color-color diagram for the K-selected galaxies and stars in the CANDELS GOODS-S (upper panel), and UDS (lower panel) fields. Arrows indicate 1σ lower limits on the measured $(B-z)$ color for sources which are undetected (S/N < 1) in the B-band. Objects shown in blue are color-selected BzK galaxies classified as "starforming" from the SED analysis. Those plotted in red are color-selected BzK galaxies classified as passively evolving with the same criterion. The red dashed line is a fixed reference to show the position of stars in the BzK plane, useful to show the consistency of photometric calibration.
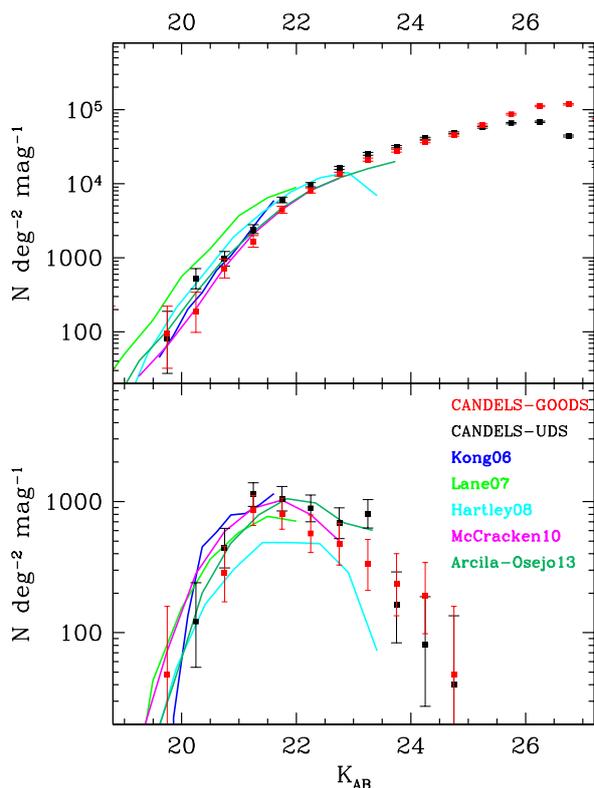
Fig. 2. Number counts for the $sBzK$ (upper panel) and $pBzK$ (bottom panel) galaxies in the two CANDELS fields plotted separately, red GOODS-S and black UDS. We assume Poissonian error bars, computed with the Gehrels (1986) formula for low number counts. Previous results from the literature are over-plotted: Kong et al. (2006) in blue, Lane et al. (2007) in green, Hartley et al. (2008) in cyan, McCracken et al. (2010) in magenta, and Arcila-Osejo et al. (2013) in dark-green.

number counts for the $sBzK$ extends well below $K \simeq 27$, where they are however significantly plagued by incompleteness in the detection. Since we are interested here in the $pBzK$ population, that is limited at much brighter magnitudes by incompleteness due to color selection, as we shall quantify below, we have made no attempt to correct for the detection incompleteness in the faintests bins of the $sBzK$ counts.

As far as $sBzK$ galaxies are concerned, our number counts are in reasonable agreement with most of the previous studies, encompassing the range of densities found by previous works, that typically were conducted over much larger areas. Probably the most striking difference is with respect to Lane et al. (2007), whose counts are above our own (and all the others). As proposed by McCracken et al. (2010), this difference could be due to an inappropriate transformation to the Daddi et al. filter set. However, we also note that they have been obtained over the UDS region. As shown in Figure 2, our counts in the UDS region are also above those in the GOODS-S region. It is therefore possible that some of this excess is due to a true overdensity of galaxies in the UDS field, where indeed a large number of $z \simeq 1.6$ galaxies within a high-density structure has been ob-

served (Papovich et al. 2010; Tanaka et al. 2010). We also note that the mismatch between our two field is close to the limit of what can be accounted for by a straightforward application of clustering statistics. Looking for instance at $sBzK$ galaxies with $K \le 22$, we find 151 and 248 galaxies in the GOODS-S and UDS fields, respectively. Using the Cosmic Variance Calculator (Trenti & Stiavelli 2008) to estimate their expected variance and converting their density to the same area of one square degree, we find that their densities are 3600 ± 596 galaxies per square degree and 5015 ± 707 galaxies per square degree, repectively, hence discrepant at the $2-3\sigma$ level.

Focusing our attention on the main subject of the current paper, the number densities of $pBzK$ galaxies in the two fields match the observed number densities from the literature in the bins where we have good statistics. There is some discrepancy with previous works, especially with McCracken et al. (2010) and Kong et al. (2006). This difference may be due to cosmic variance, given the strong clustering of pBzK galaxies with respect to $sBzK$ galaxies. There is also a systematic difference between our two fields: in total, we identify 134 $pBzK$ galaxies in the UDS and 81 in GOODS-S: even in this case, the UDS field seems overdense. Following the Cosmic Variance Calculator as described before, this translates into a number density of

1930 ± 380 and 2710 ± 440 in the GOODS-S and UDS field, respectively, that is still consistent within 2σ.

3.2. The redshift distribution of BzK galaxies

Both the UDS and the GOODS-S fields have been the target of extensive spectroscopic surveys in the past. Using these publicly available data we have first verified the accuracy and completeness of the *BzK* selection criteria in selecting galaxies in the redshift range $1.4 < z < 2.5$, expoiting a sample that is significantly larger than the original K20 sample used by Daddi et al. (2004). This is shown in Figure 3, where we plot the position of all sources with spectroscopic redshift $z_{spe} > 1$ in the *BzK* diagram; each symbol refers to a different redshift range. Figure 3 also shows the distribution of the spectroscopic redshifts of these *BzK*–selected galaxies. The significant overlap between the $1.4 < z < 2.5$ galaxy population and the *BzK* selection criterion is immediately evident. More quantitatively, we find that within the spectroscopic sample, 318 galaxies (38 & 280 in the UDS and GOODS-S, respectively) fall in the *sBzK* region. Of these, 225 (23 & 202) are at $1.4 \leq z \leq 2.5$). The total number of *pBzK* galaxies with spectroscopic redshifts is 15 (1 & 14), with only two of them outside of the $1.4 \leq z \leq 2.5$ redshift range. Conversely, 56 galaxies (2 & 54) at $1.4 \leq z \leq 2.5$ are not in the overall *BzK* region. Based on these numbers we conclude that the completeness of the *BzK* selection criterion is about 80%, and the purity around 70%. We have also verified that these numbers drop very significantly as soon as we move below $z = 1.4$ or above $z = 2.5$. This comparison confirms that the *BzK* criterion is a very effective method to select galaxies in the specific redshift range $1.4 < z < 2.5$

Despite the extensive spectroscopic coverage, for 95% of our *BzK* sample we must rely on the accurate photometric redshifts to estimate rest-frame properties like stellar mass. The resulting picture is shown in Figure 4, where we plot both the photometric redshift as well as the stellar mass of all *BzK* galaxies as a function of their *K* magnitude (the two fields are shown together). It is easily appreciated that most of the *pBzK* galaxies have photometric redshifts below $z = 2$, with a $z_{med} \simeq 1.8$, while the distribution of *sBzK* spans a wider range with $z_{med} \simeq 1.9$. The redshift distribution of the passively-evolved galaxies is in good agreement with the one presented in McCracken et al. (2010). We note that the peak of galaxies around $z \sim 1.6$ could be related to large-scale structures known in both UDS (Papovich et al. 2010; Tanaka et al. 2010) and GOODS-S fields (Castellano et al. 2007; Kurk et al. 2008).

The central point of Figure 4, however, is the evidence that the majority of the faint *pBzK* galaxies - those at $K > 23$ - are located at $z_{phot} > 2.5$, at variance with the brighter $K < 23$ sample, that are as expected at $1.4 < z < 2.5$. We have individually inspected these sources and found that their photometry is not corrupted, and their photometric redshifts are reasonably well constrained. We note that the presence of passively evolving galaxies in the *pBzK* region is not in contradiction with the expectations of synthesis models: the BC03 spectral library described before predicts that also passively evolving galaxies at $z > 2.5$ may also be located in the *pBzK* area.

It is also interesting to look at the stellar mass estimates for the *BzK* population. As shown in the upper panel of Figure 4, both *pBzK* and *sBzK* follow a general trend between the *K*-band and the stellar mass $M_\odot$. Indeed, Daddi et al. (2004) derived an average relation between *K*-band magnitude and the stellar mass, of the form: $log(M_\star/10^{11} M_\odot) = -0.4(K^{tot} - K^{11})$, where $K^{11} = 21.35$ (AB) is the *K*-band magnitude corresponding on
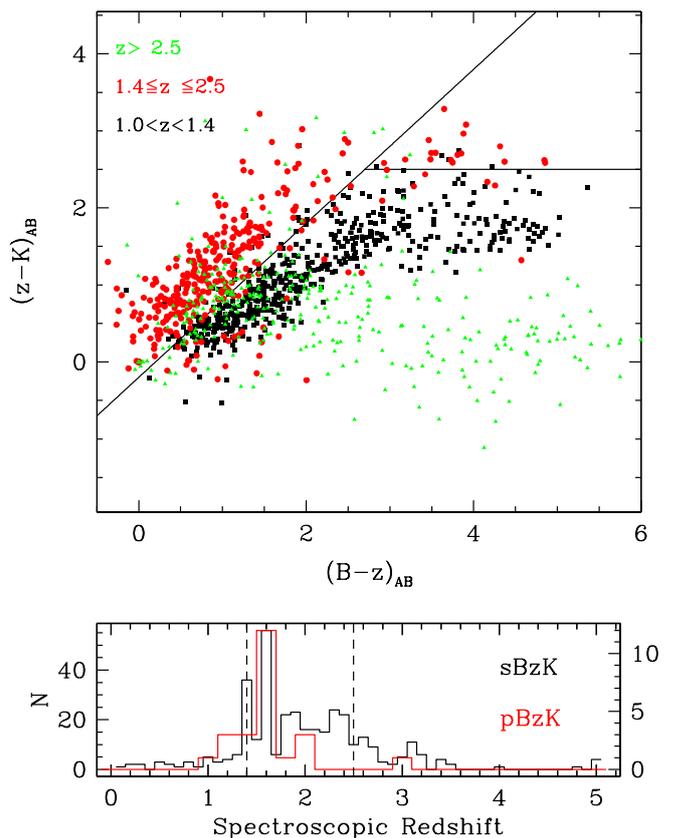

Fig. 3. *BzK* with spectroscopic redshift. *Upper panel:* Position of all galaxies with $z_{spe} > 1$ on the *BzK* plane. Each symbol refers to a different redshift range, as shown in the legend. *Lower panel:* The spectroscopic redshift distribution for the *BzK* galaxies, divided between *sBzK* and *pBzK*, as shown in the legend. The vertical dashed lines represent the canonical redshift range of *BzK* galaxies.

average to a mass of 10^{11} M$_\odot$. This was calibrated on the stellar mass estimates derived from full SED fitting in the K20 spectroscopic sample (Fontana et al. 2004), i.e. on galaxies with K_{AB}-magnitude less than 22, where exactly the same numerical code adopted here was used to estimate masses, although a previous version of the BC03 code was adopted. This is shown as a green thick line in Figure 4. The superior quality and spectral extension of the CANDELS imaging data gives us the opportunity of revising such relation. While the Daddi et al. (2004) relation seems to fairly represent the correlation for bright sources, we find that it systematically overpredicts the stellar mass for fainter sources; this is consistent with expectation considering that faint *sBzK* are typically low-mass star-forming galaxies, whose M/L is expected to be lower than more massive, evolved galaxies.

It is interesting to note that the faint *pBzK* galaxies that we locate at $z > 2.5$ are significantly offset from the general relation, as expected since they are at considerably larger redshifts.

4. Estimating the systematic effects

4.1. Incompleteness

As is evident by looking at Figure 2, the number counts of *pBzK* galaxies drop at fainter magnitudes beyond $K \simeq 21.5$. Since this is the main focus of the present paper, before analyzing it in more
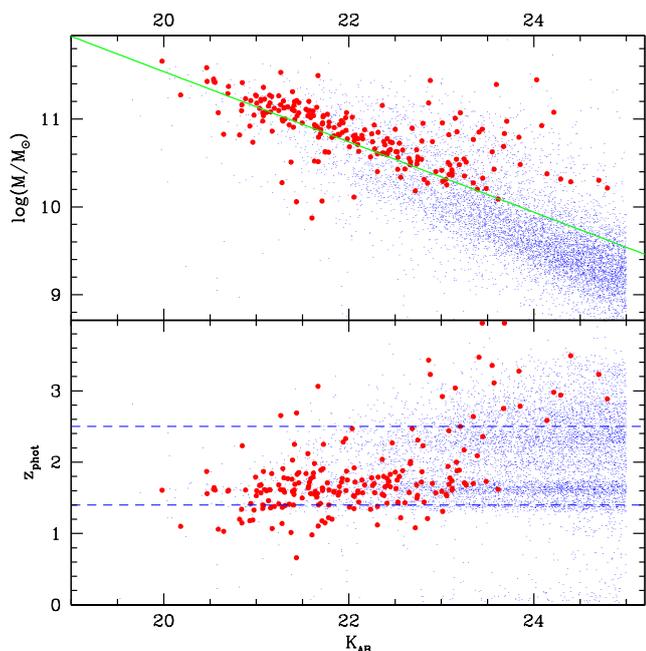
Fig. 4. Distribution of photometric redshift and stellar masses (upper panel) as a function of the K magnitude for the whole BzK sample. Blue small points refer to $sBzK$ galaxies, red dots to $pBzK$. In the lower panel the two dashed lines represent the nominal redshift range of the BzK distribution; in the upper panel, the green thick line represents the average $M_\odot - K$ relation of Daddi et al. (2004).

Table 2. Observed Number Counts of $sBzK$ and $pBzK$ galaxies in the UDS and GOODS-S fields, separately. The total averaged number counts, including also a completeness correction, are given in Table 3. The first column shows the center of each 0.5 mag bin.

K_{AB}	$N_{sBzK-UDS}$	$N_{sBzK-GOODS}$	$N_{pBzK-UDS}$	$N_{pBzK-GOODS}$
17.75	0	1	0	0
18.25	0	1	0	0
18.75	0	0	0	0
19.25	0	0	0	0
19.75	2	2	0	1
20.25	13	4	3	0
20.75	24	15	11	6
21.25	60	35	28	18
21.75	149	93	26	17
22.25	239	169	22	12
22.75	404	282	17	10
23.25	625	441	20	7
23.75	778	586	4	5
24.25	1012	776	2	4
24.75	1207	945	1	1
25.25	1421	1302	0	0
25.75	1623	1816	0	0
26.25	1690	2342	0	0
26.75	1089	2471	0	0

detail it is important to exclude the possibility that this behavior is due to systematics in the data. As already discussed in Sect. 2, we can exclude that blending is a major cause of photometric errors, or that image inhomogeneities are a major source of incompleteness. It is certainly possible, however, that this effect is due to photometric scatter. The photometric scatter could be

potentially troublesome in the case of the B band, which ultimately limits our $pBzK$ selection at the faint end. To properly measure the $B - K$ color of a galaxy at the center of the $pBzK$ region (e.g. with $(B - z) = 4$ and $(z - K) = 3$) the B band must be deep enough to allow the detection of the object as much as $\simeq 7$ magnitudes fainter than the K-band magnitude of the object. Given the depth of our B-band ($B \simeq 30$ mag.) we expect that incompleteness is already important at $K \simeq 23$. Previous analyses were done using B-band images about 2 magnitudes shallower, and we can therefore expect these effects to have been in place at even brighter magnitudes in those surveys. To further verify this, we performed simulations that are described below.

The effects of noise and incompleteness can impact in various ways the observed distribution of galaxies in the BzK plot. First, photometric noise may scatter galaxies within the BzK diagram: in particular galaxies that lie close to the lines that define the selection criteria can migrate in or out of the selection windows. In the case of the horizontal line at $z - K > 2.5$ the exquisite depth of the CANDELS and HUGS data is crucial to keep these effects to a minimum. For instance, at $K = 24$ in the GOODS-S field the typical error on the K-band magnitude is $\simeq 0.05$ mag, and the color term $z - K = 2.5$ is measured with a total error of typically 0.2 mag (we emphasize that all the $pBzK$ galaxies are detected in the z-band). The diagonal selection line is more affected by the depth of the B-band image. Again, the depth of the B band (the 1σ detection limit is $B \simeq 30$ in both fields) ensures detection also in the B-band for a large fraction of the $pBzK$ galaxies down to $K = 24$. Those undetected are shown as arrows in Figure 1: those lying outside the $pBzK$ region could be in principle bona-fide $pBzK$ galaxies scattered out because of the inadequate depth of the B-band.

Clearly, the opposite effect may also happen: galaxies located outside the boundaries of the $pBzK$ criterion can enter the region because of photometric noise and be included in the $pBzK$ galaxy sample. In order to quantify these effects in our samples, we performed a dedicated set of simulations. The ultimate goal is to define a robust limiting magnitude in the K-band, and to correct a-posteriori the observed number counts for *incompleteness* (i.e. the fraction of true $pBzK$ galaxies lost due to noise) and *contamination* (i.e. the fraction of galaxies selected by the $pBzK$ criterion that were instead originally located outside it) .

The procedure that we followed is described in Figure 5. To estimate the incompleteness, we started from the sample of observed $pBzK$ galaxies, using the brightest part of the catalog, where observational errors are so small that they do not contribute significantly to the observed scatter. After inspection of the error budget in the input catalogues, we decided to use for this purpose all objects with $K < 22$. Similarly, we use the observed catalog of objects with $K < 22$ and located in a region around the $pBzK$ boundary to estimate the amount of contamination in our sample. This sample is shown in the upper panel of Figure 5, where we plot the distribution of the objects used as input in the BzK plane, that is slightly different in the two fields. We show both the galaxies selected as input $pBzK$ galaxies (big dots) as well as those lying immediately out of the $pBzK$ region (small dots) used to estimate the contamination.

We use these objects to generate mock catalogs of 10^5 objects for each field, normalized at various K-band magnitudes from $K = 20$ to $K = 25.5$. The computed magnitudes (in all bands) are then perturbed assigning them a noise consistent with the observed error-magnitude relation in each band and field. Our simulations accurately reproduce not only the average S/N as a function of magnitude, but also its scatter in order to match

as closely as possible the observed and simulated data (Castellano et al. 2012).

Both these catalogs are then analyzed in a similar way to the ones derived from the observations. The output of this exercise is shown in the central panel of Figure 5, where we plot the position of the simulated catalogs after applying the noise, for *pBzK* galaxies only, in the case of two reference magnitudes ($K = 22$ and $K = 23.7$). For simplicity we plot only the GOODS-S field.

This plot clearly shows the effect of the finite depth of our observations. As galaxies become fainter, there is some scatter across the $z - K = 2.5$ boundary, that is however relatively small. By far the larger effect is the migration of objects toward smaller $B - z$, onto the clear locus of galaxies with undetected B-band flux. This effect is clearly dependent on the object flux and removes a significant fraction of objects from the *pBzK* region. Similar results (not shown in the figure) are found regarding the contamination - here the primary effect is due to photometric noise that causes objects close to the boundaries to enter the *pBzK* region.

The final results are shown in the lower panel of the same Figure 5, where we plot both the completeness and the contamination as a function of the K-band magnitude. They have been computed separately for the two fields, that have slightly different depths in the various bands. We find that the incompleteness obviously increases with increasing magnitude, being relatively small ($< 20\%$) up to $K = 22.5 - 23$ but reaching a level of 50% at about $K = 23.5$ for UDS and $K = 24$ for GOODS-S. In the following we will therefore focus our analysis on the $K < 24$ sample, and simply present our results down to $K = 25$, warning the reader that incompleteness corrections are very severe at $K > 24$. The contamination also increases at the faint end of our sample, reaching 20-25% at $K \simeq 24$. We will use these curves in the following to correct our number counts.

4.2. Spectral classification

We have also compared the galaxies selected with the simple color selection criteria to the output of a full SED analysis, performed on the multi-wavelength catalogs obtained from CANDELS. To understand the limitations of the *BzK* selection criterion, derived only from observed colors, we follow a different approach based on the spectral fitting technique. One simple test to verify the validity of the *BzK* criterion is to analyze the population of *BzK* galaxies by correlating the age t, the star-formation timescale τ and the dust extinction $E(B - V)$ derived from the SED fitting technique already described in Sec. 2.3.

As in Grazian et al. (2007), for each galaxy we compute the t/τ parameter, and we characterize as star-forming the galaxies with $t/\tau < 4$, and as passively-evolving those with $t/\tau \geq 4$.

Therefore, we first verify that the classification based on the t/τ parameter is consistent with the results obtained using the *BzK* criteria, i.e. we compute this parameter for all the *BzK* galaxies, and for all of them we examine the correlation between t/τ and the extinction. We verify that both star-forming and quiescent galaxies have the expected value of t/τ, as well as for the extinction. As shown in Fig. 1, there is a general consistency between the position in the *BzK* plane and the result of the SED fitting (we remind that the latter is obtained over 18-19 bands, not only on 3 as in the *BzK* case). Those located in the *pBzK* region are mostly fitted with passively evolving models, while those located in the *sBzK* area are fitted with star–forming models. This supports our conclusion that a relatively low number of *pBzK* galaxies are scattered out of the *pBzK* region because of limited depth of the *B*-band imaging.
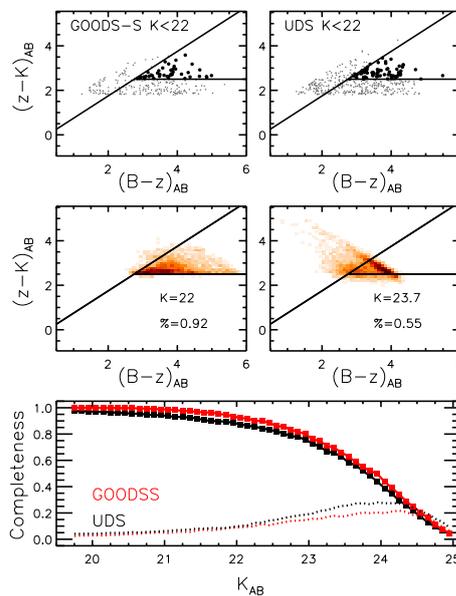
Fig. 5. Simulations used to estimate the completeness in the selection of *pBzK* galaxies. *Upper panel:* Position of the sources used to estimate the incompleteness in the two fields, taken as real *pBzK* galaxies at $K < 22$. *Central panels:* Example of the density of simulated sources in the *BzK* plane, when sources are scaled to $K = 22$ (left) and $K = 23.7$ (right), and the effect of noise is included (see text for details). The case of GOODS-S is shown in this example. *Lower panel:* Big dots delineate the completeness (i.e. the fraction of objects originally located in the *pBzK* region that are recovered even when the appropriate photometric noise is included) as a function of the *K*-band magnitude resulting from the full simulations, separately for the two fields. The small dots show the contamination, i.e. the fraction of objects detected in the *pBzK* region that were originally located outside the same region.

5. Passively evolving BzK galaxies: luminosity and mass distribution

Armed with full characterization of the selection function, we are now in a position to explore the properties of the *pBzK* galaxies. Figure 6 presents the *K*-band number counts of the *pBzK* galaxies in the CANDELS fields. In addition to the raw counts, averaged over the two fields, we present the number counts corrected for incompleteness, up to $K = 24$. For this purpose each galaxy of magnitude K in the sample has been summed as $[1 - contamin(K)]/complet(K)$, where $contamin(K)$ and $complet(K)$ are the contamination and completeness as defined above and shown in the lower panel of Figure 5. Error bars are Poissonian and computed as described above. For comparison, we also overplot the number counts found by Kong et al. (2006), Lane et al. (2007), Hartley et al. (2008), and McCracken et al. (2010), that were not corrected for incompleteness. The
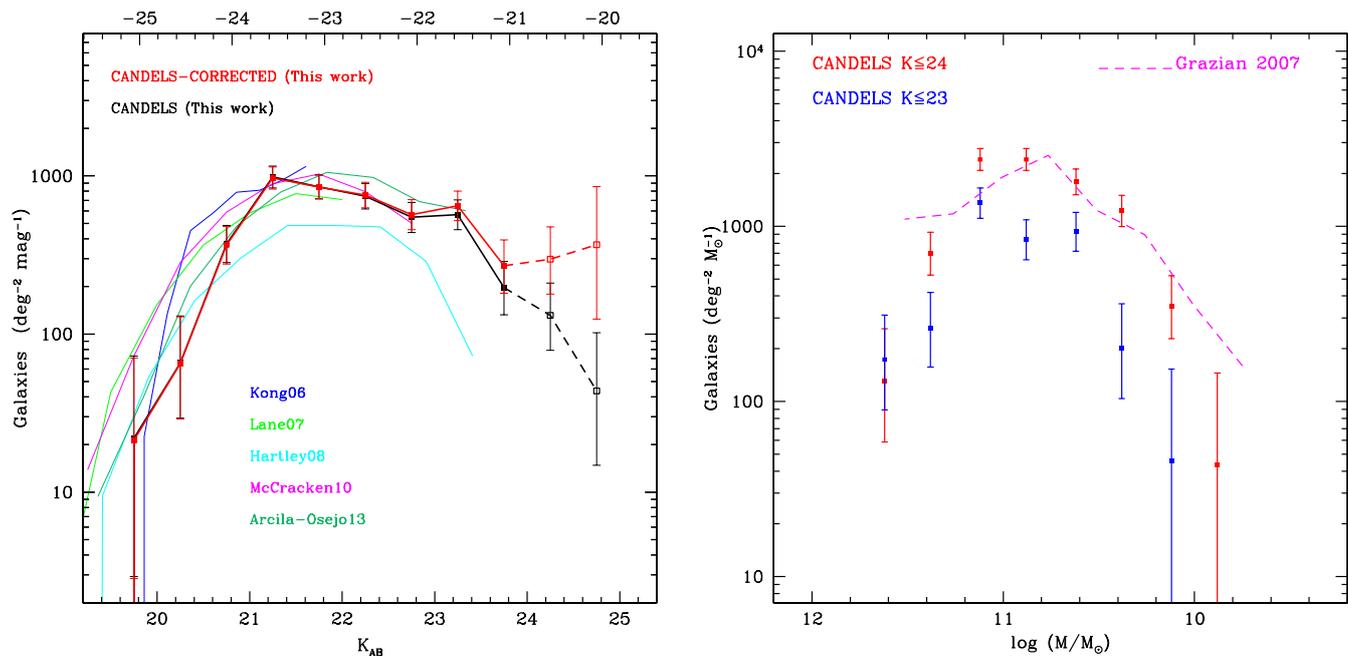
Fig. 6. *Left*: The number counts of the CANDELS (UDS+GOODS-S) *pBzK* galaxies as a function of the observed K magnitude. The black points and line show the raw data, while the red points and line show the data after correcting for incompleteness as discussed in the text. The upper x-axis shows the corresponding rest-frame absolute magnitude in the *I* band at $z \simeq 2$. As highlighted in the text, the corrections for incompleteness are below a factor 2 at most up to $K \simeq 24$, that sets the limit for a rigorous analysis. However we plot the faint end of the distribution until $K < 25$ with a dotted line for reference. The blue, green, cyan, magenta and darkgreen lines show the number counts for *pBzK* galaxies from the literature, from Kong et al. (2006), Lane et al. (2007), Hartley et al. (2008), McCracken et al. (2010), and Arcila-Osejo et al. (2013) respectively. *Right*: The stellar mass distribution of the CANDELS *pBzK* galaxies, after correction for incompleteness and contamination as described in the text. Masses are obtained with the multi-band SED-fitting technique. Blue points are obtained from the $K < 23$ sample, where all galaxies are at $z < 2.5$, while the red points are from the $K < 24$ sample, that includes also objects up to $z \simeq 3.5$. For comparison we plot also the galaxy stellar mass distribution of the *pBzK* derived by Grazian et al. (2007) from the GOODS-MUSIC sample (magenta dashed line).

number counts are in good agreement with previous studies at faint magnitude.

The *pBzK* galaxy number counts derived from our CAN-DELS (UDS+GOODS-S) sample are summarized in Table 3.

When the correction is applied, the observed number counts still show a flattening at $K > 21$, consistent with past studies (e.g. Hartley et al. 2008). The turn-over at $K \simeq 22$ is still present, although somewhat less significant. Converting these magnitudes to average rest-frame magnitudes in the *I* band, (which is sampled by the *K* band at $z \simeq 1.9$, close to the average redshift of *pBzK* galaxies with spectroscopic redshift) this corresponds to absolute magnitudes of $M_I \simeq -23$ and $M_I \simeq -22$, respectively, as shown by the upper x-axis in Figure 6 .

To further investigate the physical significance of this trend, we translate the galaxy photometry into stellar mass. We compute the stellar masses using our SED fitting to the full multi-wavelength catalogs available for the two fields, computed as described in Sections 2.3 and 4.2. We remind the reader that we adopt here a Salpeter IMF.

Figure 6 shows the resulting distribution of the stellar masses for the *pBzK* galaxy sample computed with the SED fitting technique. As shown in Figure 4, the majority of *pBzK* galaxies at $K > 23$ appear to lie at $z > 2.5$, at variance with those at $K < 23$. We therefore plot separately the distribution at $K < 23$ and at $K < 24$.

For comparison, we overplot the results obtained by Grazian et al. (2007), that were obtained from the *pBzK* sample in the (less deep) GOODS-MUSIC sample using the same SED fitting technique. The two results are quite consistent.

Table 3. Differential Number Counts for *sBzK* and *pBzK* averaged over the (UDS+GOODS-S) fields. The first column is the center of the bins. The remaining columns are in units of log(N/deg²/mag) . The last column shows the *pBzK* counts after correction for incompleteness and contamination, as described in the text.

K_{AB}	N_{sBzK}	N_{pBzK}	N_{pBzK}^{Corr}
19.75	$1.817_{0.35}^{0.30}$	$1.340_{0.87}^{0.52}$	$1.327_{0.87}^{0.52}$
20.25	$2.570_{0.12}^{0.12}$	$1.817_{0.35}^{0.30}$	$1.813_{0.35}^{0.30}$
20.75	$2.920_{0.08}^{0.08}$	$2.570_{0.12}^{0.12}$	$2.563_{0.12}^{0.12}$
21.25	$3.304_{0.05}^{0.05}$	$2.993_{0.07}^{0.07}$	$2.987_{0.07}^{0.07}$
21.75	$3.696_{0.03}^{0.03}$	$2.931_{0.07}^{0.07}$	$2.930_{0.07}^{0.07}$
22.25	$3.935_{0.02}^{0.02}$	$2.871_{0.08}^{0.08}$	$2.879_{0.08}^{0.08}$
22.75	$4.165_{0.02}^{0.02}$	$2.738_{0.10}^{0.09}$	$2.755_{0.10}^{0.09}$
23.25	$4.354_{0.01}^{0.01}$	$2.755_{0.09}^{0.09}$	$2.811_{0.09}^{0.09}$
23.75	$4.461_{0.01}^{0.01}$	$2.294_{0.17}^{0.16}$	$2.431_{0.17}^{0.16}$
24.25	$4.579_{0.01}^{0.01}$	$2.118_{0.22}^{0.20}$	$2.473_{0.22}^{0.20}$
24.75	$4.661_{0.01}^{0.01}$	$1.641_{0.47}^{0.37}$	$2.565_{0.47}^{0.37}$
25.25	$4.760_{0.01}^{0.01}$		
25.75	$4.860_{0.01}^{0.01}$		
26.25	$4.924_{0.01}^{0.01}$		
26.75	$4.873_{0.01}^{0.01}$		

The observed distribution shows that there is a clear decrease in the number density of passively evolving galaxies at stellar masses below $10^{10.8}$ M$_\odot$. This trend departs significantly from the overall form of the galaxy stellar mass function at this red-

shift, which continues to rise steeply to much lower masses (e.g. Ilbert et al. 2013). We stress that this implies that the fraction of *pBzK* galaxies compared to all *BzK* galaxies, and hence to most of the galaxies at $z \simeq 2$, is large (~25%) at $M_* \simeq 10^{11}$ M$_\odot$ and becomes minimal (~1%) at $M_* \simeq 10^{10}$ M$_\odot$.

6. Comparison with semi analytical models of galaxy formation

In the previous sections we have highlighted the existence of a clear break in the luminosity and mass distribution of passive galaxies at $z \simeq 2$, with these objects becoming progressively rarer beyond an observed *K*-band magnitude of $K \simeq 22$. This turnover in the number counts can be translated into a mass threshold roughly placed around $10^{10.8}$ M$_\odot$. This implies that the mechanisms that halted star formation in galaxies at high redshift have been more efficient (or statistically more frequent) in massive galaxies rather than in lower mass ones. It is interesting to investigate whether this basic feature is reproduced by theoretical models of galaxy formation.

We concentrate on four Semi-Analytical Models (SAMs): Menci et al. (2008), Merson et al. (2012) (based on the SAM of Bower et al. 2006), Somerville et al. (2012), and Lu et al. (specifically, in the best fit case of the rendition described in Lu et al., 2013; see also Lu et al. 2011, 2012).

These models vary both in the way they assemble the dark matter halos as well as in the prescriptions adopted for the various physical mechanisms involved in galaxy formation. Here we briefly mention the physical processes relevant in the discussion of our result. We refer the reader to the original papers for full details of the models, and outline here only the major differences. In the Menci model the merging histories of dark matter haloes are described through Monte Carlo simulations, the Merson model uses dark matter merger histories extracted from the Millenium simulation (Springel et al. 2005), while the Somerville and Lu models use the Bolshoi N-body simulations (see Klypin et al. 2011 for details). We note that the resolution of these N-body simulations in practice sets a lower limit to the mass (hence luminosity) of the smaller galaxies traced in the simulations, and hence to the depth of the luminosity distributions that we are presenting. Different modes for the suppression of gas cooling in massive halos are implemented in the SAMs, either by artificially turning off the cooling of hot gas in haloes above a tunable mass threshold (as implemented in the Lu model), or through the inclusion of a specific model for AGN feedback. The latter can be either related to the active AGN phase (quasar mode), or ignited by the continuous accretion of gas in dark matter haloes undergoing quasi-hydrostatic cooling (radio mode). The quasar mode is implemented in both the Somerville and in the Menci model, which both assume the AGN activity to be triggered by galaxy interactions: the latter can be constituted only by galaxy merging (as in the Somerville model) or include also galaxy fly-by (as in the Menci SAM). The radio mode AGN feedback is implemented in the Merson and in the Somerville model, and influences galaxies with massive black holes at the center of massive haloes.

All these models provide simulated galaxy samples, for which magnitudes in any desired filter set are given. The Somerville and Lu models provide lightcone mock catalogs that mimic the geometry of the UDS and GOODS-S fields, while the other two average over larger areas of the sky. Galaxy magnitudes are computed from the predicted star formation and chemical enrichment histories using single stellar population model

(SSP). All these models use the SSP model of Bruzual & Charlot (2003) but they assume a different initial mass function (IMF): Kennicutt IMF (Merson), Salpeter IMF (Menci), Chabrier IMF (Somerville and Lu). We do not correct the luminosities and colours for the different IMF because the parameters of each model have been tuned to reproduce observations.

The dust extinction affecting the above magnitudes is computed from the dust optical depth and applying the appropriate attenuation to the luminosity at various wavelengths. The only exception is the Lu et al. model that does not include dust extinction.

For all these models we have extracted the *BzK* magnitudes and applied exactly the same *BzK* criterion we applied to real data, as described in the previous sections.

First of all we have tested whether these models are able to reproduce the passive galaxies selected by the *pBzK* criterion. To this aim, Figure 7 shows the distribution of model galaxies at $1.4 < z < 2.5$ in the *BzK* plane in two bins of *K* magnitude, one corresponding to *K* magnitudes below the observed peak in the number counts at $K \simeq 21.5$, the other corresponding to fainter magnitudes. The gray-scale shows the average specific SFR (SSFR) at a given position in the *BzK* plane, in decades ranging from quiescent galaxies (SSFR=10^{-13}yr^{-1}) to actively star-forming (SSFR=10^{-9}yr^{-1}). All models reproduce the distribution of galaxies in the *BzK* diagram reasonably well. On average, the SSFR of galaxies populating the upper right region of the *B-z* versus *z-K* colour plane is lower than it is in those populating the *BzK* star forming region (*BzK* ≥-0.2). In the case of the Menci model there is a somewhat large fraction of objects slightly outside the *BzK* region, but this is still consistent with the expected color evolution of galaxies at various ages in the redshift range $1.4 < z_{phot} < 2.5$ (Daddi et al. 2004). The Lu et al. model is devoid of bright *sBzK* galaxies in the reddest region ($(B-z) \simeq (z-K) \simeq 2$); this region is mostly populated by dusty star-burst galaxies, and hence this deficit is expected, considering that the Lu et al. model does not include a prescription for dust absorption. In particular, in all models, the *pBzK* criterion selects galaxies with SSFR<10^{11}yr^{-1} which is well below the inverse of the Hubble time at $z = 2$ ($1/t_{Hubble}$=3×10^{-10}yr^{-1}), thus the selected *pBzK* galaxies are actually passive (see e.g. Franx et al. 2008; Fontana et al. 2009).

In any case, most models predict that some fraction of the population of passive galaxies at $z \simeq 2$ is actually located outside the classical *pBzK* region, such that present observations might be missing a whole class of objects in the color-color plane. As shown in Daddi et al. (2004), and in Grazian et al. (2007), the *pBzK* selection criterion preferentially selects galaxies that have been passively evolving for about 1 Gyr: lowering the threshold in $(z-K)$ corresponds to introducing passive galaxies that are progressively younger, and hence become more numerous. Hence, we should expect that lowering this threshold would also increase the number of observed galaxies. Unfortunately this cannot be easily checked in the data, since lowering the threshold in $(z-K)$ immediately introduces also galaxies at lower redshift that contaminate the selection.

This allows us to turn back to our central result, concerning the decrease in the number density of passive galaxies at faint luminosities. We compare in Figure 8 the predicted and observed number counts of *pBzK* galaxies as a function of *K* magnitude. Since the observations of *pBzK* galaxies are severely affected by incompleteness, we decided to follow a twofold approach. In the upper panel we plot the comparison between the observed data and the theoretical data, including the effect of incompleteness in the theoretical data only: the catalog produced by the theoretical

models has been convolved with the instrumental noise as in the simulations used for estimating the completeness. In the lower panel we have plotted the data corrected for incompleteness and the theoretical models with no correction. As expected the two approaches provide us with a consistent picture, with the latter giving us also the opportunity to show what the models predict at magnitudes fainter than our survey.

We first note that two models, Merson et al. (2012) and Somerville et al. (2012), exhibit a global trend that is *qualitatively* consistent with the observed break in the luminosity distributions. Their predicted number density reaches a peak at $K \simeq 21.5$ similar to what we observe in the real data, and decreases at fainter magnitudes. However, they overpredict the absolute number density of the passive galaxies at faint magnitudes. By contrast, the Menci and the Lu models perform poorly both at large and at small masses. They underestimate the number of massive passive galaxies, do not even predict a turn-over. In both cases the number counts continue to increase exponentially towards fainter magnitudes (i.e. to lower stellar masses).

These discrepancies highlight that some of the prescriptions adopted to describe the main baryonic processes lead to noticeable differences among the various models and in some case need a substancial revision. We remark that our criterion is effective to select galaxies that are undergoing a passive phase since at least $\simeq 1$ Gyr, already at $z \simeq 2$: this allows us to test the implementation of physical processes that not only quench the star–formation process but also prevents it from starting again after a relatively short time. In general terms, the formation of passive galaxies depends on several proceess, like: the efficiency of gas cooling and star–formation rate, the ejection of gas out of galaxies (due for instance by AGN and stellar feedback) and processes that deplete their gas reservoir (like stripping of cold gas in halo merging). A higher efficiency in the star–formation process and a lower feedback lead to a fast transformation of the gas content of a given halo into stars: in the absence of further cooling or in the presence of stripping of hot gas during halo merging, this processes makes galaxies quiescent. On the contrary, lower efficiencies and higher feedback with subsequent cooling eventually lead to much more extended (albeit intermittent) epochs of star-formation, making galaxies bluer. While these trends are common to all models, their specific implementation varies among them, leading to the differences that we observe.

At the bright magnitudes the differences in model predictions can be interpreted in terms of the AGN feedback, that is often identified as a potentially major factor in the quenching of star-formation activity, and is suspected to be more effective in massive galaxies. Based on this comparison, we can speculate that the radio mode feedback seems to be more efficient in producing bright passive galaxies than the QSO mode and halo quenching model.

At the faint magnitudes ($K \lesssim 23$) all models over-estimate the number of passive objects. This is directly related to the well-known tendency of hierarchical clustering scenarios to produce steep luminosity functions (see e.g. Somerville & Primack 1999; Cole et al. 2000; Menci et al. 2002; Benson et al. 2003). Hierarchical clustering scenarios predict the high-redshift progenitor galaxies to be characterized by low virial temperature and high densities, making the gas cooling extremely efficient at $z \gtrsim 3$; the short dynamical time scales and the frequent merging events rapidly convert such available cold gas into stars. In the absence of competing effects, the rapid star formation in low-mass galaxies at $z \gtrsim 3$ would result in an excess of red low-mass galaxies already at $z \simeq 2$, where our survey is sensitive.

Another physical process that is very important in predicting the number of faint red galaxies is the stripping of the hot gas reservoir of galaxies residing in subhaloes. All models, indeed, assume that when a halo merges with a larger halo (becoming a subhalo) its hot gas content is stripped away. The galaxy residing in the sub-halo rapidly consumes its cold gas reservoir and thereafter becomes red and passively evolving. This is particularly effective in dense environments at intermediate and high redshift. The current implementation of such a mechanism produces an excess of red faint galaxies in all theoretical models developed so far. This aspect was explored at low redshift by Weinmann et al. 2006, comparing a SAM model to the observations from the SDSS survey. Guo et al. 2011 modified the implementation of the process in the model in order to delay the stripping of hot gas after halo merging. Even in this case, however, the excess of faint red galaxies is not completely removed. Other, more exotic possibilities have been also explored: for instance, Nierenberg et al. 2013 have shown that, by adopting a Warm Dark Matter power spectrum, the number of satellite galaxies is significantly reduced.

There is no doubt that this excess is at least partly responsible for the excess of predicted galaxies that we observe at low masses in the *pBzK* population. For this reason Merson et al. (2012) made the test of removing the satellite galaxies altogether from the predicted counts of *pBzK*, finding a good agreement with the observed counts. This is clearly an indication that this process is involved in the overestimate. In the case of the Menci and Lu models the discrepancy at faint luminosities is much larger, despite the fact that gas stripping is included in a very similar fashion, suggesting that other processes are also involved. Unfortunately, it is impossible to make a more accurate test of the relative contribution of central and satellite galaxies, since some fraction of the observed data are also satellite galaxies: given that extended large scale structures are detected in both our fields in the redshift range of *BzK* galaxies, this fraction could be substantial. This remains a clearly important test to be executed that deserves a dedicated analysis of the data (both in field surveys as well as in high redshift clusters).

7. Summary and Discussion

In this paper we have exploited new deep, wide-field K-band imaging, performed with the High Acuity Wide field K-band Imager (HAWK-I) on VLT as part of the HAWK-I UDS and GOODS-S survey (HUGS; VLT Large Program), to study the population of passive evolving galaxies at $z \sim 2$. Crucially, both survey fields possess B and z-band imaging, as well as a wealth of other multi-wavelength data, extending from the U-band to the mid-infrared *Spitzer*, and containing deep HST imaging assembled as part of the CANDELS HST Treasury program.

To define a sample of star forming and quiescent galaxies at redshift between $1.4 < z < 2.5$, we use the *BzK* criterion proposed by Daddi et al. (2004). Thanks to the depth of our observations, we have now extended the selection to magnitudes fainter than was possible in previous analysis. At bright magnitudes the observed number counts of the *sBzK* and *pBzK* galaxies are in good agreement with previous studies, in particular with McCracken et al. (2010) as shown in Figure 2.

In particular we focus on passively evolving galaxies, i.e. the so called *pBzK* galaxies. We find a total of 101 *pBzK* galaxies in the UDS CANDELS field, and 89 in the GOODS-S field. We have demonstrated through simulations that – in our deep sample – the statistics of passive galaxies down to $K \simeq 22.5$ are not significantly affected by incompleteness, and that the latter
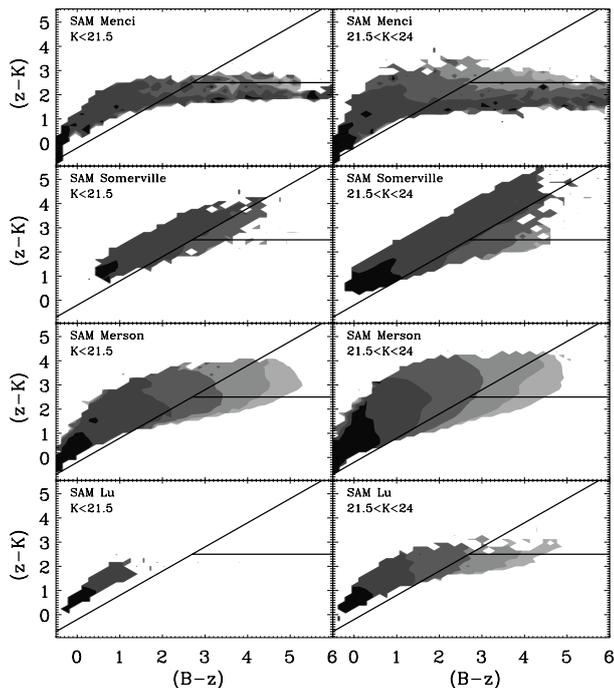
Fig. 7. *B-z* versus *z-K* colour-colour diagram for model galaxies in two bins of *K*-magnitude. The filled contours correspond to the predicted average values of the specific star formation rate of model galaxies for bins of different *B-z* and *z-K*. The SSFR values are equally spaced in logarithmic scale from SSFR=10^{-13}yr^{-1} for the lightest filled region to SSFR=10^{-9}yr^{-1} for the darkest.

Fig. 8. Number counts of *pBzK* galaxies compared with model prediction of Merson et al. (2012) in blue, Menci et al. (2008) in green, Lu et al. (2013) in black, and Somervile et al. (2012) in cyan. *Upper panel.* Mock catalogs from theoretical models (solid colored lines) are convolved with the same photometric errors and incompleteness that affect the data. Points refer to the raw observed counts, without any correction for incompleteness. *Lower panel.* Here the theoretical models are shown without any correction, while observed data are corrected for incompleteness as described in the text.

is still treatable down to $K \simeq 24$. Thanks to the depth of our observations we are now able to place on a secure footing the earlier results on the *pBzK* number counts previously reported by Hartley et al. (2008) and McCracken et al. (2010).

Our central result is that the number counts of *pBzK* galaxies show a flattening at $K_s \sim 21$, with indications of a turn-over at $K_s > 22$, equivalent to rest-frame absolute *I*-band magnitudes of $M_I = -23, -22$ respectively. Converted into stellar mass, our result corresponds to a decrease in the number density of passively-evolving galaxies at stellar masses below $10^{10.8}$ M$_\odot$ for a Salpeter IMF. As judged against the still steeply-rising number counts of the overall galaxy population at these redshifts, this turnover is fairly abrupt, indicating that at high redshift the mechanism that quenches star-formation activity is much less efficient below this mass limit.

Another central result is related to the redshift distribution of *pBzK* galaxies. As expected, nearly all *pBzK* galaxies at $K < 23$ are at $1.4 < z < 2.5$. However, at $K > 23$ a sharp transition appears to exist, with most of the *pBzK* galaxies having a redshift definitely above $z = 2.5$, typically at $2.7 < z < 3.4$. This result confirms the existence of passively-evolving galaxies at $z > 2.5$, as suggested by a number of recent papers (e.g. Fontana et al. 2009; Straatman et al. 2014).

We have compared our observed number counts with the predictions of several semi-analytical models of galaxy formation and evolution, in particular with the models of Menci et al.
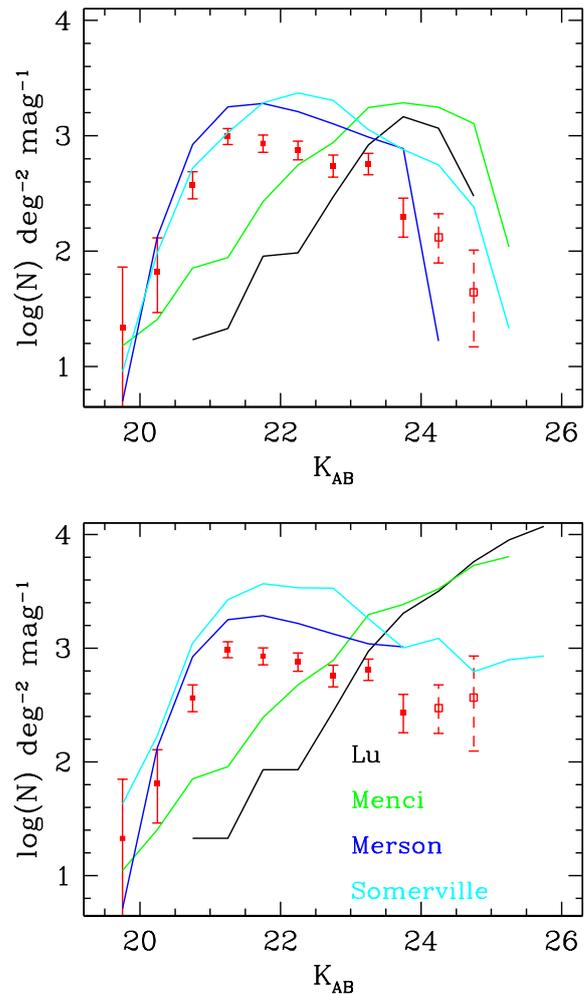
(2008), Somerville et al. (2012), Merson et al. (2013), and Lu et. al. (2011). Among these SAMs only two, (Somerville et al. (2012) and Merson et al. (2013)) *qualitatively* predict the shape of the number counts, showing a turn-over at a stellar mass close to that observed in the data, but they do not reproduce the absolute observed density of the passive galaxies. In contrast, the other two models fail to show this turn-over, and predict an exponential increase of passive objects to faint magnitudes. This comparison suggests that the distribution of number density (with magnitude or stellar mass) of quiescent galaxies at these redshifts offers a critical test for hierarchical models, and can place strong constraints on the detailed baryonic physical processes involved in galaxy formation and evolution.

The importance of this basic finding should not be underestimated. Indeed, current models of galaxy formation are able to provide acceptable fits to the observed properties of the *bulk* of

the galaxy population, such as luminosity functions or color distributions. What we show here is that the physical mechanisms that they implement are not able to correctly reproduce the *extreme* star formation histories characterizing the *pBzK* galaxy population.

The observed discrepancies raise pressing questions concerning the comparison between observations and the current models of galaxy formation in a cosmological context. First, are the current implementations of the star-formation quenching process (tuned to match the observed local luminosity functions) effective in reproducing the evolution of galaxies in the color-color plane? While at large masses the most likely candidate is the AGN feedback, at small masses stellar feedback and gas stripping in satellite galaxies are probably the main processes that produce the observed abundance of the *pBzK* population. They both need to be better understood and parametrized to provide us with a satisfactory fit to the observed number counts.

Second, is the relative role of the different star-formation modes correctly implemented in the models? In particular, it is known that both merging and disk instabilities can provide starbursts which add to the secular conversion of gas into stars (the "quiescent mode" of star formation). Current galaxy-formation models are characterized by different implementations of three modes of star formation; while the bulk of the galaxy population could be less dramatically affected by the relative role of such processes, the abundance of *pBzK* galaxies characterized by extremely early star-formation histories could be extremely sensitive to the relative importance of the different star-formation modes.

Unfortunately, it is currently not possible to determine the specific features that, within each model, produce the observed trends on the quenching of star formation. This requires a more detailed investigation that we plan to explore in a forthcoming paper.

Andreon, S., Huertas-Company, M., 2011, A&A, 526A, 11

Arcila-Osejo, L., & Sawicki, M., 2013, MNRAS, 435, 845

Blanc, G. A., Lira, P., Barrientos, L. F., et al., 2008, ApJ, 681, 1099

Bower, R., G., Benson, A., J., Malbon, R., et al., 2006, MNRAS, 370, 645

Brammer, G.B., Whitaker, K. E., van Dokkum, et al., 2011, ApJ, 739, 24

Bruzual, G., & Charlot, S., 2003, MNRAS, 344, 1000

Calzetti, D., Armus, L., Bohlin, R., C., et al., 2000, ApJ, 533, 682

Castellano, M., Fontana, A., Grazian, A., et al., 2012, A&A, 540, 39

Daddi, E., Cimatti, A., Renzini, A., et al., 2004, ApJ, 617, 746

Daddi, E., Renzini, A., Pirzkal, N., et al., 2005, ApJ, 626, 680

Dahlen, T., Mobasher, B.., and CANDELS Collaboration, 2012, AAS, 22013301D

De Lucia, G., Springel, V., White, S. D. M., et al., 2006, MNRAS, 366, 499

De Lucia, G., & Blaizot, J., 2007, MNRAS, 375, 2

De Lucia, G., Poggianti, B. M., Aragn-Salamanca, A., et al., 2007, MNRAS, 374, 809

Fioc, M. & Rocca-Volmerange, B. 1997, A&A, 326, 950

Fontana, A., Donnarumma, I., Vanzella, E., et al., 2003, ApJ, 994, 9

Fontana, A., Pozzetti, L., Donnarumma, I., et al., 2004, A&A, 424, 23

Fontana, A., Salimbeni, S., Grazian, A., et al., 2006, A&A, 459, 745

Fontana, A.,Santini, P.; Grazian, A.; et al., 2009, A&A, 501, 15

Furusawa, H., Kosugi, G., Akiyama, M., et al., 2008, ApJ, 176, 1

Galametz, A., Grazian, A., Fontana, A., et al, 2013, ApJ, 206, 10

Gehrels, N., 1986, ApJ, 303, 336

Giavalisco, M., Ferguson, H. ,C., Koekemoer, A., M., et al., 2004, ApJ, 600, 93

Grazian, A., Fontana, A., Moscardini, L., et al., 2006, 453, 507

Grazian, A., Salimbeni, S., Pentericci, L., et al., 2007, A&A, 465, 393

Grogin, N. A., Kocevski, D. D., Faber, S. M., et al., 2011, 2011, ApJS, 197, 35

Guo, Qi; White, Simon; Boylan-Kolchin, Michael; et al., 2011, MNRAS, 413, 101

Guo, Y., Ferguson, H. C., Giavalisco, M., et al, 2013, ApJS, 207, 24

Hartley, W. G., Lane, K. P., Almaini, O., et al., 2008, MNRAS, 391, 1301

lbert, O., McCracken, H., J., Le Fevre, O., et al., 2013, A&A, 556, 55I

Kitzbichler, M. G., & White, S. D. M, 2007, MNRAS, 376, 2

Klypin, A. A., Trujillo-Gomez, S., & Primack, J., 2011, ApJ, 740, 102

Kodama, T., Yamada, T., Akiyama, M., et al., 2004, MNRAS, 350, 1005

Koekemoer, A. M., Faber, S. M., Ferguson, H. C., et al., 2011, ApJS, 197, 36

Kong, X., Daddi, E., Arimoto, N., et al., 2006, ApJ, 638, 72

Lane, K. P., Almaini, O., Foucaud, S., et al., 2007, MNRAS, 379, 25

Lawrence, A., Warren, S., J., Almaini, O., et al., 2007, MNRAS, 379, 1599

Lee, K.-S., Ferguson, H. C., Wiklind, T., Dahlen, T., et al., 2012, ApJ, 752, 66

Lu, Y., Mo, H. J., Weinberg, M. D., & Katz, N., 2011, MNRAS, 416, 1949

Lu, Y., Mo, H. J., Katz, N., & Weinberg, M. D., 2012, MNRAS, 421, 1779

Lu, Y., Wechsler, R. H., Somerville, R. S., Croton, D. et al., 2013, arXiv1312.3233L

Menci, N., Fontana, A., Giallongo, E., et al, 2005, ApJ, 632, 49

Menci, N., Fiore, F., Puccetti, S., et al., 2008, ApJ, 686, 219

Merson, A. I., Baugh, C. M., Helly, J. C., et al., 2012, arXiv1206.4049

McCracken, H. J., Capak, P., Salvato, M., et al., 2010, ApJ, 708, .202

Muzzin, A., Marchesini, D., Stefanon, M., et al., 2013, arXiv1303.4409M

Nierenberg, A. M.; Treu, T.; Menci, N., et al., 2013, ApJ, 772, 146

Reddy, N. A., Erb, D. K., Steidel, C. C., et al, 2005, ApJ, 633, 748

Somerville, R. S., Gilmore, R. C., Primack, J. R., et al., 2012, MNRAS, 423, 1992

Straatman, C. M. S., Labbé, I., et al., 2014, ApJL 783, 14

Stutz, A. M., Papovich, C., & Eisenstein, D. J., 2008, ApJ, 677, 828

Trenti, M., & Stiavelli, M., 2008, ApJ, 676, 767

Weinmann, Simone M.; van den Bosch, Frank C.; Yang, Xiaohu; et al., 2006, MNRAS, 372, 1161